AD-A119 733 CORNELL UNIV ITHACA NY BAKER LAB F/G 20/7
DIFFERENTIAL SPUTTERING CORRECTION FOR ION MICROSCOPY USING IMA--ETC(U)
SEP 82 A J PATKIN, S CHANDRA, G H MORRISON N00014-80-C-0538
UNCLASSIFIED TR-10 NL

END
DATE FILMED
11-82
DTIC

(10)

OFFICE OF NAVAL RESEARCH

Contract N00014-80-C-0538

Task No. NR 051-736

TECHNICAL REPORT No. 10

DIFFERENTIAL SPUTTERING CORRECTION FOR ION MICROSCOPY USING IMAGE DEPTH PROFILING

by

Adam J. Patkin, Subhash Chandra, and
George H. Morrison*

Prepared for Publication

in

Analytical Chemistry

Cornell University
Department of Chemistry
Ithaca, N. Y. 14853

September 22, 1982

SECURITY CLASSIFICATION OF THIS PAGE (When Data Entered)

REPORT DOCUMENTATION PAGE

READ INSTRUCTIONS BEFORE COMPLETING FORM

1. REPORT NUMBER: Technical Report No. 10	2. GOVT ACCESSION NO.: AD-A119733
3. RECIPIENT'S CATALOG NUMBER:	
4. TITLE (and Subtitle): DIFFERENTIAL SPUTTERING CORRECTION FOR ION MICROSCOPY USING IMAGE DEPTH PROFILING	5. TYPE OF REPORT & PERIOD COVERED: Interim Technical Report
	6. PERFORMING ORG. REPORT NUMBER:
7. AUTHOR(s): A. J. Patkin, Subhash Chandra, and G. H. Morrison	8. CONTRACT OR GRANT NUMBER(s): N00014-80-C-0538
9. PERFORMING ORGANIZATION NAME AND ADDRESS: Department of Chemistry, Cornell University, Ithaca, N. Y. 14853	10. PROGRAM ELEMENT, PROJECT, TASK AREA & WORK UNIT NUMBERS: NR051-736
11. CONTROLLING OFFICE NAME AND ADDRESS: ONR (472), 800 N. Quincy St., Arlington, VA 22217	12. REPORT DATE: September 22, 1982
	13. NUMBER OF PAGES: 23 pages
14. MONITORING AGENCY NAME & ADDRESS (if different from Controlling Office):	15. SECURITY CLASS. (of this report): Unclassified
	15a. DECLASSIFICATION/DOWNGRADING SCHEDULE:

16. DISTRIBUTION STATEMENT (of this Report)

Approved for public release: distribution unlimited

17. DISTRIBUTION STATEMENT (of the abstract entered in Block 20, if different from Report)

18. SUPPLEMENTARY NOTES

Prepared for publication in ANALYTICAL CHEMISTRY

19. KEY WORDS (Continue on reverse side if necessary and identify by block number)

SIMS, Secondary Ion Microscopy, Ion Microscopy, MIDAS, SIMS-IDP, DISCOR, Differential Sputtering Correction, Digital Image Processing, Biological Tissue, Raphanus sativus, Radish

20. ABSTRACT (Continue on reverse side if necessary and identify by block number)

A first-order correction for differential sputtering is made to ion micrographs using image depth profiling. This is done by first recording the ion image to be corrected, then sputtering down to the substrate while recording a series of images at the substrate's mass. A time-domain "burn-through" map showing the time each location of the sample first sputters through to the substrate is then generated. This map is used to make a linear correction for differential sputtering induced ion intensity artifacts to the initial sample images. $^{40}Ca^{+}$ ion images of a radish root tip stele cell region on a tantalum substrate are

DD FORM 1 JAN 73 1473

SECURITY CLASSIFICATION OF THIS PAGE (When Data Entered)

corrected in this fashion. Relative sputtering rates of 1.5 and 1.2 compared to the cytoplasm were found for the cell walls and nuclei, respectively.

DIFFERENTIAL SPUTTERING CORRECTION FOR ION MICROSCOPY USING IMAGE DEPTH PROFILING

Adam J. Patkin, Subhash Chandra, and George H. Morrison *

Department of Chemistry
Baker Laboratory
Cornell University
Ithaca, New York 14853

BRIEF: Image depth profiling is used to determine relative sputtering rates of features in plant tissue analyzed by ion microscopy. Corrections for differential sputtering are made to the ion micrographs.

DIFFERENTIAL SPUTTERING CORRECTION FOR ION MICROSCOPY USING IMAGE DEPTH PROFILING

Adam J. Patkin, Subhash Chandra, and
George H. Morrison *

Department of Chemistry
Baker Laboratory
Cornell University
Ithaca, New York 14853

BRIEF: Image depth profiling is used to determine relative sputtering rates of features in plant tissue analyzed by ion microscopy. Corrections for differential sputtering are made to the ion micrographs.

Ion microscopy, a form of secondary ion mass spectrometry (SIMS), is an analytical technique with the ability to generate mass resolved images of a solid sample with elemental detection limits at the parts per million level (1). A 2-20 keV primary ion beam is used to sputter the top atomic layers of the sample and secondary ions emitted from this region are extracted and mass-analyzed to produce ion images. Qualitative interpretations of ion images have been shown to be useful in studies of elemental distributions in biological tissues (2-8). However, quantitative interpretations of ion images can be erroneous because of the problem of differential sputtering, a phenomenon first pointed out by Galle (9) and more recently by Farmer, et al (10).

The observed SIMS secondary ion intensity may be described by the equation of Morrison and Slodzian (1):

$$I = \tau C_m S i_p a_o \qquad (1)$$

where I is the measured secondary ion current, τ the practical ion yield, C_m the atomic concentration of the element M (corrected for its isotopic abundance), S the total sputtering yield (number of atoms of any kind removed per incoming particle), i_p the number of primary particles arriving per unit time and unit area on the target surface, and a_o is the analyzed area on the target surface.

Local variations in composition across a spatially heterogeneous sample's surface cause different regions of the sample to sputter at different rates. Since the observed intensity I is proportional to S, this causes erroneous ion intensity enhancements, and therefore higher apparent elemental concentrations, for the more rapidly sputtered regions. Biological tissue is a very heterogeneous material, and is thus particularly prone to differential sputtering.

An appropriate correction for differential sputtering is therefore needed for any type of quantitative work for biological tissue in particular, and spatially heterogeneous materials in general.

This paper demonstrates a first-order differential sputtering correction using digital image processing. It is performed by mounting a thin biological sample upon a substrate which produces secondary ions at a mass not observed in the sample. Images at masses of interest are recorded from the sample. The sample is then sputtered down to the substrate while a series of ion images is recorded, with increasing depth, at the substrate's mass by the image depth profiling (IDP) method of Patkin and Morrison (11). A "burn-through" map is generated from the IDP images, recording the time each location of the sample sputtered down to the substrate. This time-domain burn-through map is then used to correct the initial sample ion images for differential sputtering induced ion intensity artifacts.

EXPERIMENTAL SECTION

Instrumentation: Ion images were obtained with a CAMECA IMS-3f ion microscope. This ion microscope obtains images at selected mass/charge ratios which retain the original spatial relationships of the elements in the sample (12).

The microscopic image digital acquisition system (MIDAS) (13) shown in Fig. 1 was used to record images. MIDAS consists of a low-light level ISIT (intensified silicon intensified target) T.V. camera, digital frame buffer (digitally stores a 256 x 240 x 12-bit image), analog/digital converter, computer, graphics display screen, and associated computer software. The T.V. camera is focused upon the fluorescent screen

of the ion microscope. The images are acquired by the T.V. camera/frame buffer and stored by the computer. Changes from the original MIDAS description (13) include replacement of the CAMECA IMS-300 ion microscope with more sophisticated CAMECA IMS-3f and dedicated H.P. 9845T microcomputer, replacement of the DEC PDP-11/20 minicomputer and GT-40 graphics display terminal with a DEC PDP-11/34A with 256K byte RAM and two 10M byte disks, and the use of a f/2.0, 102-mm zoom lens on the T.V. camera set at 40 mm for a 50 μm field-of-view.

Computer Software: Programs were written in FORTRAN IV, RATFOR (a structured FORTRAN IV pre-processor), and MACRO-11 assembly language.

There are four stages for differential sputtering correction by image depth profiling and digital image processing; acquisition of the image data, amendment of the data for detector and SIMS induced artifacts, image display, and the calculation of the relative differential sputtering rates of various sample features. Five separate but related programs were used for these functions.

IMAGE performs T.V. image acquisition, disk input/output of images, image display and registration.

GRFTDK acquires a series of images and transfers them to disk storage at an operator defined rate of up to one image every eight seconds.

DETCOR corrects images for spatial inhomogeneities in the image detector system. This is performed by acquiring a standard image of a smooth Si <100> single crystal, with the IMS-3f immersion lens optics slightly defocused to provide a uniformly intense ion image. The MIDAS output image is influenced by non-uniform detector response and degradation so that it appears inhomogeneous. DETCOR determines the correction factor at each pixel necessary to bring that pixel's intensity up to the maximum intensity of

the standard image, correcting for detector system heterogeneity. It then uses this factor to correct the current elemental image.

GCONV converts raw image intensities to the corresponding ion intensity using an empirically derived calibration equation.

DISCOR generates the burn-through map and then uses it to correct the image for differential sputtering. This is done by initially setting each pixel of the map to zero. The substrate images acquired by GRFTDK are then sequentially analyzed and the burn-through map updated as follows:

$$I^{m}_{x,y} = \begin{cases} & \text{current value} & \text{next value} \\ 0 & 0 & 0 \\ 0 & > 0 & 0 \\ T & 0 & > 0 \\ \text{current value} & > 0 & > 0 \end{cases}$$

where $I^{m}_{x,y}$ is the new value of the pixel located at x,y in the burn-through map, current value is the value currently stored in that location of the burn-through map and next value is the intensity at location x,y of the image currently being examined in the GRFTDK depth profile sequence. T is the sputtering time at which the GRFTDK image being examined was acquired.

Simply, this functions as follows: Since the substrate on which the sample is mounted is being imaged, any pixel with a non-zero intensity indicates the sample has been completely sputtered away at that location. To avoid spurious readings, however, the program waits until a location

gives a continuous series of non-zero substrate ion intensities in the IDP sequence before assigning that location a burn-through time. The burn-through time assigned is the time at which the first of these images was acquired. This procedure is repeated for every image in the IDP sequence, ultimately yielding the burn-through map which contains the time at which each pixel first sputtered through to the substrate.

At this point the burn-through map is used to perform a linear correction to the observed image intensities of the elements of interest in the sample such that:

$$I^{c}_{x,y} = I^{i}_{x,y} \cdot \frac{\text{burn-through time}}{\text{total sputtering time}}$$

where I^{c} is the differential sputtering corrected image, and I^{i} is the detector discrimination corrected and ion intensity converted elemental image This gives an ion image corrected, at least to a first approximation, for differential sputtering effects. This correction is based on two assumptions. The first is that the observed secondary ion intensity is proportional to the sputter rate. The second assumption requires that a given region of the sample sputters at a uniform rate throughout the course of the analysis.

Analytical Procedure: The IMS-3f instrumental conditions are shown in Table I. The parameters were chosen to optimize image quality, intensity, and sample sputtering rate. The time between images was chosen on the basis of the primary ion beam species and sample thickness.

Sample Preparation: Root tips of Raphanus sativus (radish) seedlings were selected for the study because of their well defined intracellular calcium distribution. One to 2-mm pieces of root tips were chemically fixed for 1 hr. using 5% gluteraldehyde in 0.03 M Pipes buffer [piperazine N-N^{1}bis,(2-ethanol sulfonic acid)] at pH 6.8 (14). Root tips were washed with 0.15 Pipes buffer and then postfixed for 1 hr. in 1% osmium tetroxide in the same buffer. After dehydration in ethanol (70-90%) and propylene oxide, the tissue pieces were embedded in low viscosity resin (15). Sections were cut on distilled water using a LKB Ultrotome III and transferred onto a polished tantalum disk. Tantalum was selected as a substrate because it was not expected to be present in tissue. Sections were then stored under vacuum until analyzed in the ion microscope.

RESULTS AND DISCUSSION

Calcium in plant root tip cells was chosen for analysis due to its well defined intracellular distribution (16). A light micrograph of the stele cell region of a radish root tip section is shown in Figure 2. Figure 3 is a $^{40}Ca^{+}$ ion micrograph clearly showing higher intensity of calcium in nuclei and cell walls than in cytoplasm. The severity of differential sputtering is indicated by Figure 4. This is not an image of $^{40}Ca^{+}$, but of the substrate, $^{181}Ta^{+}$, taken in the course of the image depth profile. These features clearly show that differential sputtering causes the nuclei and cell walls to sputter away well before the cytoplasm region. This is a serious effect which must be considered in any quantitative work.

Figure 5 is a typical burn-through map, with the lighter areas indicating the locations requiring the longest time to sputter away. The map clearly shows the cell walls as the most rapid sputtering features followed by the nuclei and then the cytoplasm. This root tip section was 0.5 μm thick and took ~5 minutes to completely burn through to the substrate.

Figure 6 presents the raw $^{40}Ca^{+}$ ion image and the same image after detector discrimination, ion intensity conversion and differential sputtering corrections. Both images have been normalized to the same maximum intensity. Significant differences in the distribution of calcium in the tissue are observed and the corrected image more accurately indicates the presence of calcium in the respective features, especially in the cytoplasm. This image more closely demonstrates the physiological distribution expected in the in vivo situation.

Quantitatively there has been a change in the relative intensities of different features. This will obviously affect the results when converting finally from ion intensity to concentration.

The relative feature sputtering rates R_f can be calculated once the burn-through map has been generated by ratioing the average burn-through times of different features. Table II contains the average R_f values and corresponding standard deviations for cell walls and nuclei in the stele cell region of radish root tip cells under both Ar^{+} and O_2^{+} bombardment. The sputter rates have been normalized to the cytoplasm sputter rate, the slowest sputtering feature.

The R_f values indicate that differential sputtering makes cell walls appear to have 1.5 times and nuclei 1.2 times more calcium (or any other element) than cytoplasm. Like results have been observed in our laboratory with corn and pea root tip cells. Galle (9) has also reported nuclei to sputter faster than cytoplasm in frog nucleated red blood cells.

The differentially sputtering nature of biological tissue may be due to its heterogeneous chemical composition. In the case of plant cells, cell wall is primarily composed of polysaccharides (cellulose, hemicellulose, pectine, etc.), while the nucleus is basically a proteinous material rich in DNA (deoxyribonucleic acid), RNA (ribonucleic acid), nucleoproteins, and histone proteins.

A burn-through map at a substrate mass also revealed that epoxy (where tissue is not present) was the last to sputter through, (i.e., after cytoplasm). This helps to explain the influence of epoxy in the differential sputtering of epoxy-infiltrated biological tissue. In the case of plants, cell walls are denser material than nuclei and cytoplasm, hence there may be more penetration of epoxy (mass per unit area) into the less dense cytoplasm than the denser nuclei or still more dense cell walls.

It is interesting to note that both primary beam species induce similar R_f values even though in addition to the differences in reactivity of these two species the average tissue sputter rate for an Ar^+ primary beam is greater than that observed with O_2^+ primary beam.

The R_f values indicate the possibility that our assumption of uniform sputter rate with depth may not necessarily be valid, at least when section thickness exceeds 0.5 μm. The decrease of the R_f value with increasing sample thickness indicates significant sample homogenization. In fact, partial diffusion of $^{40}Ca^+$ was observed to occur after several minutes of bombardment, possibly due to local sample heating or charge induced diffusion. However, the basic sample structure appears unchanged as cellular features are well defined in the $^{181}Ta^+$ image and burn-through maps.

Factors other than differential sputtering, such as sample surface topology (17) and matrix effects (18) can also influence the observed secondary ion signal intensity, often by several orders of magnitude. Several methods of dealing with these problems have been examined elsewhere (19), and are beyond the scope of this discussion. While the influence of these factors, particularly the matrix effects, may be larger than that of differential sputtering, any comprehensive quantitation procedure will have to include corrections for differential sputtering.

In summary, differential sputtering presents a problem in the quantification of ion images, particularly for biological thin sections where cellular organelles differ widely in their chemical composition. Image depth profiling has been used to make first-order corrections for this problem. This method of correction is useful when a thin flat sample is deposited on a substrate. In addition to biological tissues this technique should also be applicable to other thin films, such as certain types of semiconductor devices and metallurgical samples.

ACKNOWLEDGEMENT

The authors wish to acknowledge the help of William C. Harris, Jr. in manuscript preparation.

LITERATURE CITED

(1) Morrison, G. H.; Slodzian, G. Anal. Chem. 1975, 47, 932A-943A.

(2) Spurr, A. K. Scanning Electron Microscopy 1980, 3, 97-109.

(3) Frostell, G.; Larsson, S. J.; Lodding, A.; Odelius, H.; Peterson, L. G. Scand. J. Dent. Res. 1977, 85, 18-21.

(4) Burns- Bellhorn, M. S.; Lewis, R. K. Exp. Eye Res. 1976, 22, 505-518.

(5) Burns-Bellhorn, M. S.; File, B. M. Anal. Biochem. 1979, 92, 213-221.

(6) Galle, P. Ann. Phys. Biol. Med. 1970, 4, 83-94.

(7) Truchet, M. J. Micro. Biol. Cell. 1975, 24, 1-21.

(8) Campbell, N. A.; Stika, K. M.; Morrison, G. H. Science 1979, 204, 185-187.

(9) Galle, P. Symp. Microprobe Anal. as Applied To Cells and Tissues, Battelle Res. Center, Seattle, Pub. Acad. Press, London, 1973, 89-105.

(10) Farmer, M. E.; Linton, R. W.; Ingram, P.; Sommer, J. R.; Shelburne, J. D. J. Micros. 1981, 124, RP1 - RP2.

(11) Patkin, A. J.; Morrison, G. H. Anal. Chem. 1982, 54, 2-5.

(12) Ruberol, J. M.; Leqpareu, M.; Autier, B.; Gourgout, J. M. VIII Inter. Cong. on X-Ray Optics and Microanal. and the 12th Ann. Conf. of the Microbeam Analysis Society, Boston, Mass., 1977, 133A-133D.

(13) Furman, B. K.; Morrison, G. H. Anal. Chem. 1980, 52, 2305-2310.

(14) Salema, R.; Brandao, I. J. Submicr. Cytol. 1973, 5, 79-96.

(15) Spurr, A. R. J. Ultrastr. Res. 1969, 26, 31043.

(16) Chandra, S.; Chabot, J. F.; Morrison, G. H.; Leopold, A. C. Science, 1982 (In press).

(17) Cheney, K. B.; Pitkin, E. T. J. Appl. Phys. 1965, 36, 3542-3544.

(18) Castaing, Raymond; Slodzian, Georges J. Microscopy, 1962, 1, 395-410.

(19) Morrison, G. H. in Secondary Ion Mass Spectrometry, SIMS III, eds. A. Benninghoven, et al, 1982, 244-256.

CREDIT

Funding for this project was provided by the National Institutes of Health, the National Science Foundation, and the Office of Naval Research.

Table I. Instrumental Operating Conditions

Primary Ions	Ar^+, O_2^+
Primary ion energy	10 keV
Primary ion current	3.6×10^{-4} A/cm^2
Sputtered area of sample	5.6×10^{-5} cm^2
Secondary ion polarity	positive
Transfer optics	150 μm
Vacuum at sample	3×10^{-8} torr
Image field-of-view	50 μm
Image integration period	2 seconds
Time between images	8-40 seconds

Table II. Average R_f Values by Section Thickness

Primary Beam	Cellular Feature	R_f values 0.25 µm thick section	0.50 µm thick section	1.0 µm thick section
Ar^+	R_f cell walls	1.51 ± 0.22	1.46 ± 0.04	1.19 ± 0.06
	R_f nuclei	1.20 ± 0.04	1.16 ± 0.02	1.09 ± 0.06
O_2^+	R_f cell walls	1.30 ± 0.08	1.50 ± 0.02	1.17 ± 0.01
	R_f nuclei	1.18 ± 0.13	1.18 ± 0.04	1.15 ± 0.01

FIGURE CAPTIONS

Figure 1. System configuration

Figure 2. Light micrograph of radish root tip stele cell region (nu = nucleus, cw - cell wall, cy = cytoplasm)

Figure 3. $^{40}Ca^{+}$ ion micrograph of stele cells (nu = nucleus, cw = cell wall, cy = cytoplasm)

Figure 4. $^{181}Ta^{+}$ ion micrograph of substrate 150 seconds into image depth profile

Figure 5. Time-domain burn-through map

Figure 6. Comparison of original elemental ion image and same image after detector discrimination, ion intensity conversion, and differential sputtering corrections.

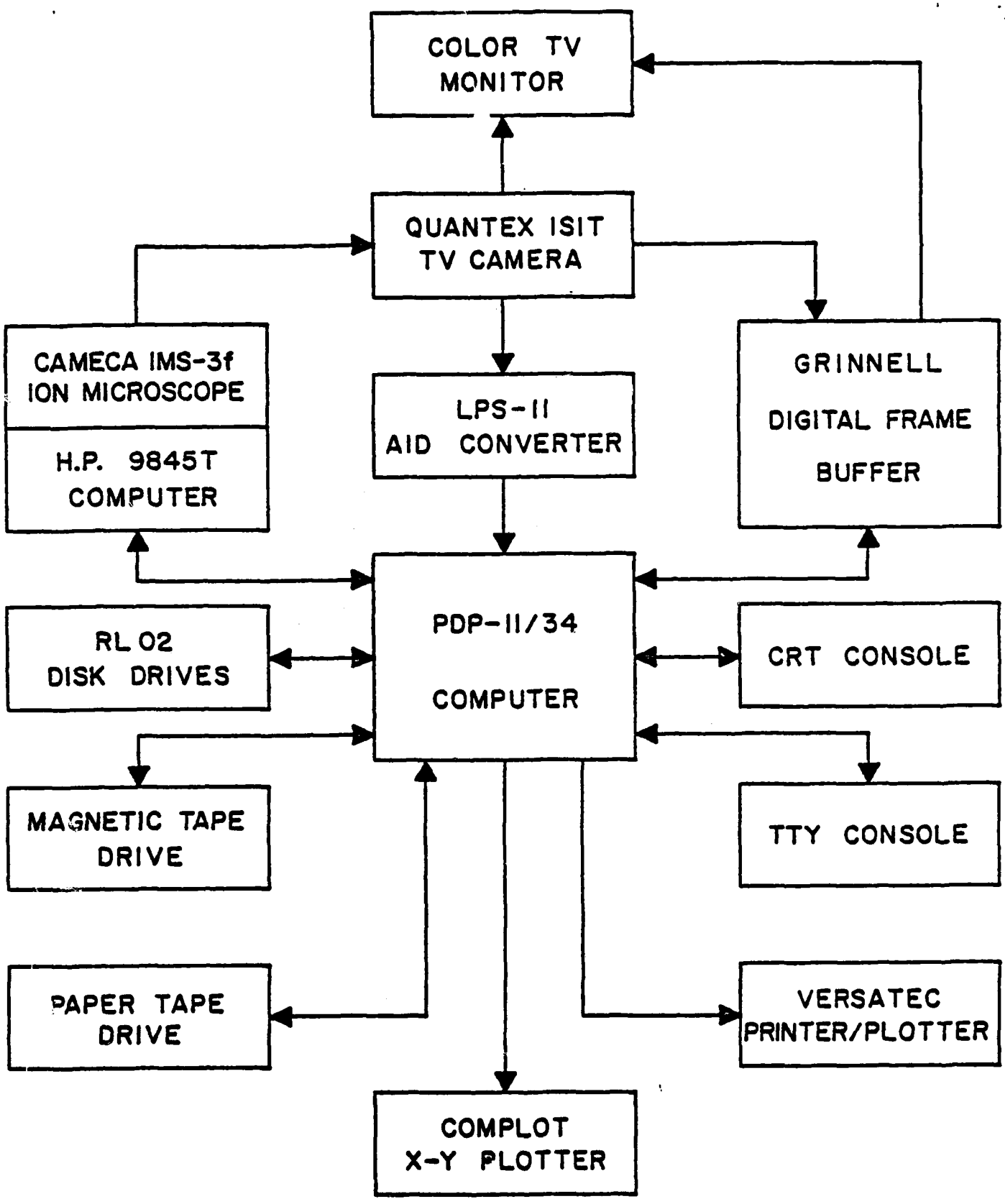

SYSTEM CONFIGURATION

cy
mu
cw

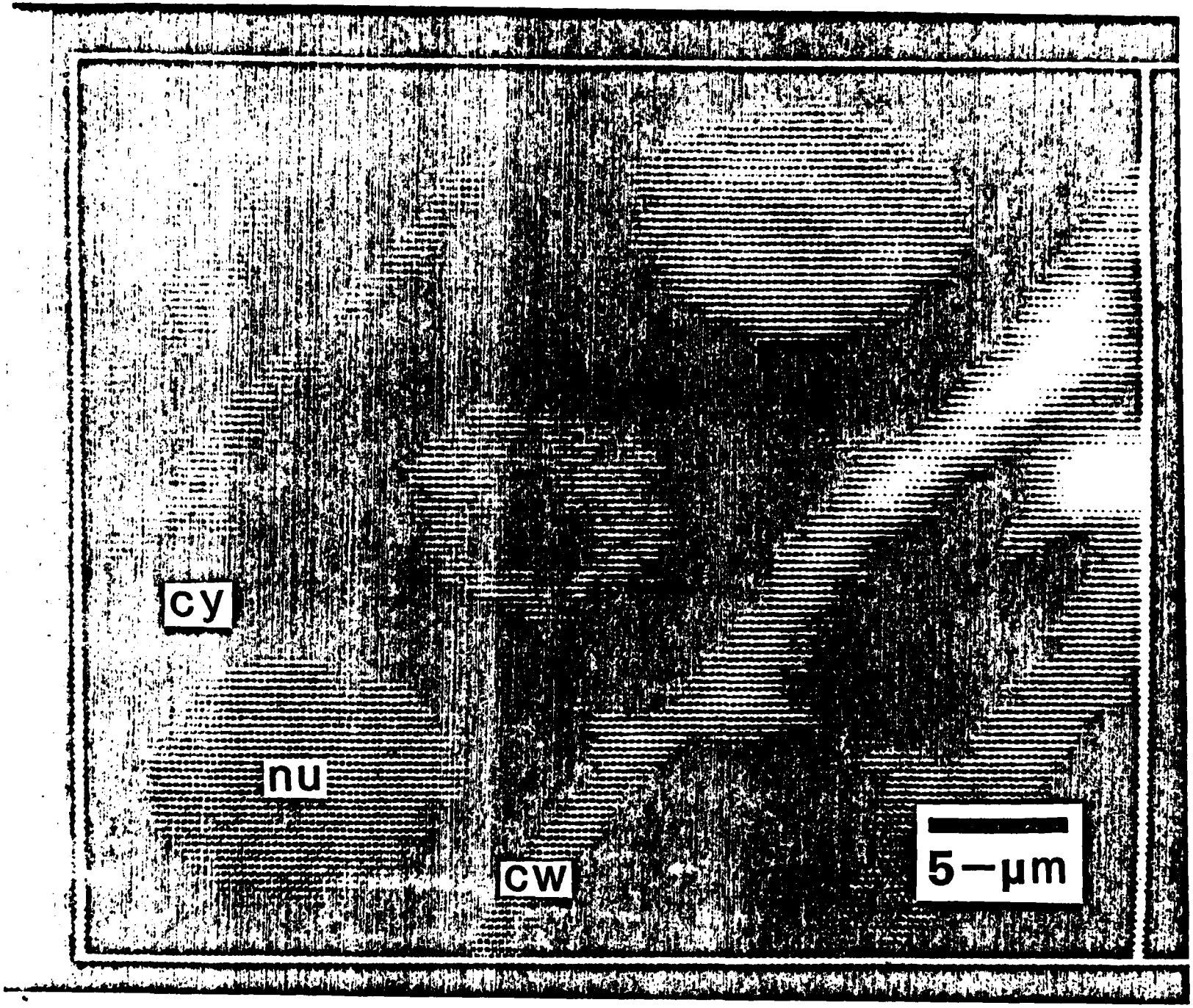
cy
nu
cw
5–µm


IMAGE DEPTH PROFILE - 150 SEC
181 T A +

RESULTS OF DETECTOR SYSTEM AND DIFFERENTIAL SPUTTERING CORRECTIONS

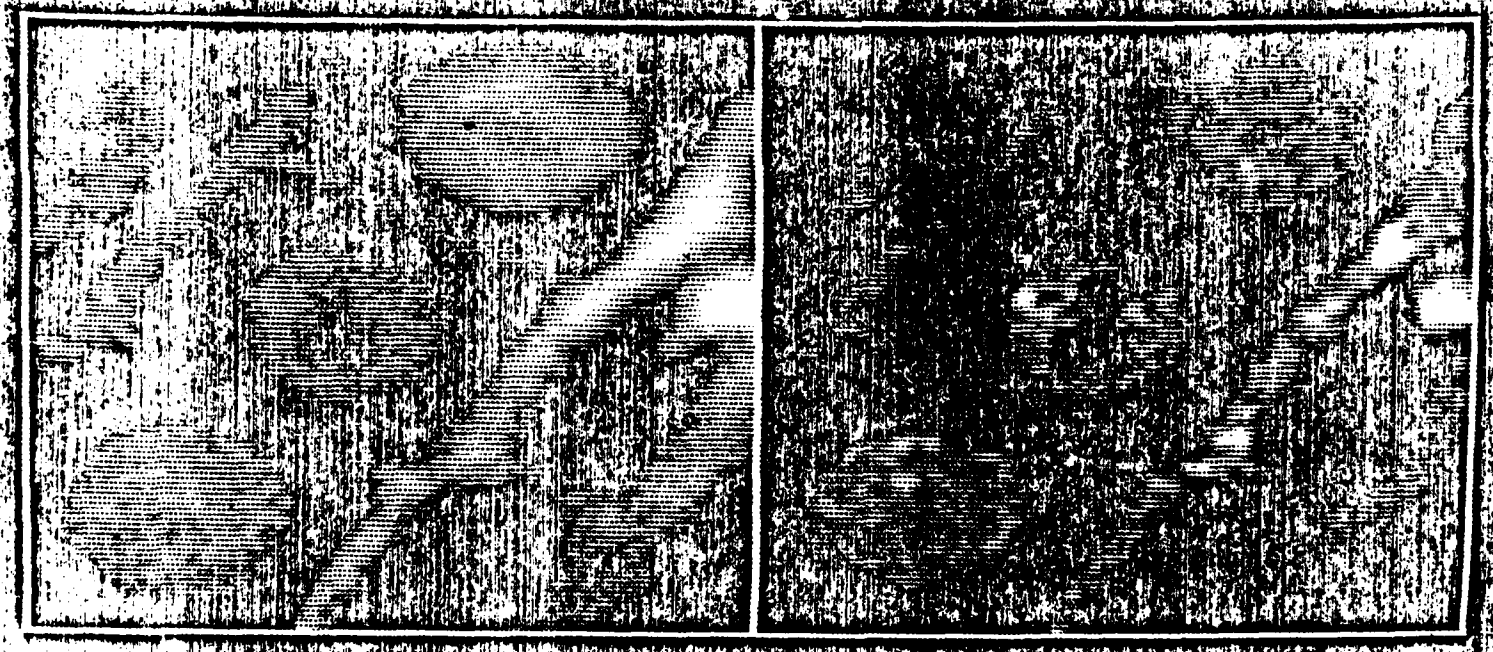

ORIGINAL

CORRECTED

TECHNICAL REPORT DISTRIBUTION LIST, GEN

	No. Copies
Office of Naval Research Attn: Code 472 800 North Quincy Street Arlington, Virginia 22217	2
ONR Branch Office Attn: Dr. George Sandoz 536 S. Clark Street Chicago, Illinois 60605	1
ONR Area Office Attn: Scientific Dept. 715 Broadway New York, New York 10003	1
ONR Western Regional Office 1030 East Green Street Pasadena, California 91106	1
ONR Eastern/Central Regional Office Attn: Dr. L. H. Peebles Building 114, Section D 666 Summer Street Boston, Massachusetts 02210	1
Director, Naval Research Laboratory Attn: Code 6100 Washington, D.C. 20390	1
The Assistant Secretary of the Navy (RE&S) Department of the Navy Room 4E736, Pentagon Washington, D.C. 20350	1
Commander, Naval Air Systems Command Attn: Code 310C (H. Rosenwasser) Department of the Navy Washington, D.C. 20360	1
Defense Technical Information Center Building 5, Cameron Station Alexandria, Virginia 22314	12
Dr. Fred Saalfeld Chemistry Division, Code 6100 Naval Research Laboratory Washington, D.C. 20375	1
Dr. Rudolph J. Marcus Office of Naval Research Scientific Liaison Group - Amer. Embassy A.P.O. San Francisco, CA. 96503	1
U.S. Army Research Office Attn: CRD-AA-IP P.O. Box 1211 Research Triangle Park, N.C. 27709	1
Naval Ocean Systems Center Attn: Mr. Joe McCartney San Diego, California 92152	1
Naval Weapons Center Attn: Dr. A. B. Amster, Chemistry Division China Lake, California 93555	1
Naval Civil Engineering Laboratory Attn: Dr. R. W. Drisko Port Hueneme, California 93401	1
Department of Physics & Chemistry Naval Postgraduate School Monterey, California 93940	1
Dr. A. L. Slafkosky Scientific Advisor Commandant of the Marine Corps (Code RD-1) Washington, D.C. 20380	1
Office of Naval Research Attn: Dr. Richard S. Miller 800 N. Quincy Street Arlington, Virginia 22217	1
Naval Ship Research and Development Center Attn: Dr. G. Bosmajian, Applied Chemistry Division Annapolis, Maryland 21401	1
Naval Ocean Systems Center Attn: Dr. S. Yamamoto, Marine Sciences Division San Diego, California 91232	1
Mr. John Boyle Materials Branch Naval Ship Engineering Center Philadelphia, Pennsylvania 19112	1
Mr. James Kelley DTNSRDC Code 2803 Annapolis, Maryland 21402	1

SP472-3/B1

472:GAN:716:lab
78u472-608

TECHNICAL REPORT DISTRIBUTION LIST, 051C

	No. Copies
Dr. M. B. Denton Department of Chemistry University of Arizona Tucson, Arizona 85721	1
Dr. R. A. Osteryoung Department of Chemistry State University of New York at Buffalo Buffalo, New York 14214	1
Dr. B. R. Kowalski Department of Chemistry University of Washington Seattle, Washington 98105	1
Dr. S. P. Perone Department of Chemistry Purdue University Lafayette, Indiana 47907	1
Dr. D. L. Venezky Naval Research Laboratory Code 6130 Washington, D.C. 20375	1
Dr. H. Freiser Department of Chemistry University of Arizona Tuscon, Arizona 85721	
Dr. Fred Saalfeld Naval Research Laboratory Code 6110 Washington, D.C. 20375	1
Dr. H. Chernoff Department of Mathematics Massachusetts Institute of Technology Cambridge, Massachusetts 02139	1
Dr. K. Wilson Department of Chemistry University of California, San Diego La Jolla, California	1
Dr. A. Zirino Naval Undersea Center San Diego, California 92132	1
Dr. John Duffin United States Naval Postgraduate School Monterey, California 93940	1
Dr. G. M. Hieftje Department of Chemistry Indiana University Bloomington, Indiana 47401	1
Dr. Victor L. Rehn Naval Weapons Center Code 3813 China Lake, California 93555	1
Dr. Christie G. Enke Michigan State University Department of Chemistry East Lansing, Michigan 48824	1
Dr. Kent Eisentraut, MBT Air Force Materials Laboratory Wright-Patterson AFB, Ohio 45433	1
Walter G. Cox, Code 3632 Naval Underwater Systems Center Building 148 Newport, Rhode Island 02840	1
Professor Isiah M. Warner Texas A&M University Department of Chemistry College Station, Texas ~~77840~~ 77843	1
~~Professor George H. Morrison~~ ~~Cornell University~~ ~~Department of Chemisty~~ Ithaca, New York 14853	~~1~~
Professor J. Janata Department of Bioengineering University of Utah Salt Lake City, Utah 84112	1
Dr. Carl Heller Naval Weapons Center China Lake, California 93555	1
Dr. L. Jarvis Code 6100 Naval Research Laboratory Washington, D. C. 20375	1